Photo-thermal modulation of surface plasmon polariton propagation at telecommunication wavelengths

Serkan Kaya, Jean Claude Weeber, F. Zacharatos, K. Hassan, T. Bernardin, B. Cluzel, Julien Fatome, Christophe Finot

Photo-thermal modulation of surface plasmon polariton propagation at telecommunication wavelengths

S. Kaya, J.-C. Weeber,* F. Zacharatos, K. Hassan, T. Bernardin, B. Cluzel, J. Fatome, and C. Finot

LICB, UMR 6303 CNRS-Université de Bourgogne,9 Av. A. Savary, BP 47870 F-21078 DIJON, FRANCE

jcweeber@u-bourgogne.fr

Abstract: We report on photo-thermal modulation of thin film surface plasmon polaritons (SPP) excited at telecom wavelengths and traveling at a gold/air interface. By operating a modulated continuous-wave or a Q-switched nanosecond pump laser, we investigate the photo-thermally induced modulation of SPP propagation mediated by the temperature-dependent ohmic losses in the gold film. We use a fiber-to-fiber characterization set-up to measure accurately the modulation depth of the SPP signal under photo-thermal excitation. On the basis of these measurements, we extract the thermo-plasmonic coefficient of the SPP mode defined as the temperature derivative of the SPP damping constant. Next, we introduce a figure of merit which is relevant to characterize the impact of temperature onto the properties of bounded or weakly leaky SPP modes supported by a given metal at a given wavelength. By combining our measurements with tabulated values of the temperature-dependent imaginary part of gold dielectric function, we compute the thermo-optical coefficients (TOC) of gold at telecom wavelengths. Finally, we investigate a pulsed photo-thermal excitation of the SPP in the nanosecond regime. The experimental SPP depth of modulation obtained in this situation are found to be in fair agreement with the modulation depths computed by using our values of gold TOC.

OCIS codes: (240.6680) Surface plasmons; (260.3910) Metal optics; (350.5340) Photo-thermal effects.

References and links

1. G. P. Pells and M. Shiga, "The optical properties of copper and gold as a function of temperature," J. Phys. C (Solid St. Phys.) **2**, 1835–1846 (1969).
2. K. Ujihara, "Reflectivity of metals at high temperatures," J. Appl. Phys **43**, 2376–2382 (1972).
3. R. Rosei, F. Antonangeli, and U. M. Grassano, "d bands position and width in gold from very low temperature thermomodulation measurements," Surf. Sci. **37**, 689–699 (1973).
4. P. Winsemius, M. Guerrisi, and R. Rosei, "Splitting of the interband absorption edge in Au: Temperature dependence," Phys. Rev. B **12**, 4570–4572 (1975).
5. P. Winsemius, F. F. van Kampen, H. P. Lengkeek, and C. G. van Went, "Temperature dependence of the optical properties of Au, Ag and Cu," J. Phys. F: Metal Phys. **6**, 1583–1606 (1976).
6. R. Rosei and D. W. Lynch, "Thermomodulation spectra of Al, Au and Cu," Phys. Rev. B **5**, 3883–3893 (1972).
7. T. Holstein, "Theory of transport phenomena in an electron-phonon gas," Ann. Phys. **29**, 410 (1964).
8. R. N. Gurzhi, "Mutual electron correlation in metal optics," Sov. Phys. JETP **8**, 673 (1959).

#193955 - $15.00 USD Received 15 Jul 2013; revised 30 Aug 2013; accepted 4 Sep 2013; published 13 Sep 2013

9. J. A. McKay and J. A. Rayne, "Temperature dependence of the infrared absorptivity of the noble metals," Phys. Rev. B **13**, 673–685 (1976).
10. C. S. Moreira, A. M. N. Lima, H. Neff, and C. Thirstrup, "Temperature-dependent sensitivity of surface plasmon resonance sensors at gold-water interface ," Sensor and Actuators B **134**, 854–862 (2008).
11. X.-Y. Zhang, T. Zhang, A.-M. Hu, X.-J. Xue, P.-Q. Wu, and Q.-Y. Chen, "Tunable microring resonator based on dielectric-loaded surface plasmon polariton waveguides," J. Nanosci. Nanotechnol. **11**, 10 520–10 524 (2011).
12. M. Liu, M. Pelton, and P. Guyot-Sionnest, "Reduced damping of surface plasmons at low temperatures," Phys. Rev. B **79**, 035 418 (2009).
13. G. Baffou and R. Quidant, "Thermo-Plasmonics: using metallic nanostructures as nanosources of heat," Laser Photon. Rev. **7**, 171–187 (2013).
14. M. Rashidi-Huyeh and B. Palpant, "Counterintuitive thermo-optical response of metal-dielectric nanocomposite materials as a result of local electromagnetic enhancement," Phys. Rev. B **74**, 075 405 (2006).
15. B. Palpant, M. Rashidi-Huyeh, B. Gallas, S. Chenot, and S. Fisson, "Highly dispersive thermo-optical properties of gold nanoparticles," Appl. Phys. Lett. **90**, 223 105 (2007).
16. J.-S. G. Bouillard, W. Dickson, D. P. O'Connor, G. A. Wurtz, and A. V. Zayats, "Low temperature plasmonics of metallic nanosctructures," Nanolett. **12**, 1561–1565 (2012).
17. R. T. Beach and R. W. Christy, "Electron-electron scattering in the intraband optical conductivity of Cu, Ag and Au," Phys. Rev. B **16**, 5277–5284 (1977).
18. G. R. Parkins, W. E. Lawrence, and R. W. Christy, "Intraband optical condutuctivity $\sigma(\omega, T)$ of Cu, Ag, Au: Contribution from electron-electron scattering," Phys. Rev. B **23**, 6408–6416 (1981).
19. S. K. Ozdemir and G. Turhan-Sayan, "Temperature effects on surface plasmon resonance: Design considerations for an optical temperature sensor ," J. Lightwave Technol. **21**, 805 (2003).
20. A. Passian, A. L. Lereu, E. T. Arakawa, A. Wig, T. Thundat, and T. L. Ferrell, "Modulation of multiple photon energies by use of surface plasmons," Opt. Lett. **30**, 41–43 (2005).
21. A. L. Lereu, A. Passian, J. P. Goudonnet, T. Thundat, and T. L. Ferrell, "Optical modulation processes in thin films based on thermal effects of surface plasmons," Appl. Phys. Lett. **86**, 154 101 (2005).
22. T. Nikolajsen, K. Leosson, and S. I. Bozhevolnyi, "In-line extinction modulator based on long-range surface plasmon polaritons," Opt. Commun. **244**, 455–459 (2005).
23. G. Gagnon, N. Lahoud, G. Mattiussi, and P. Berini, "Thermally activated variable attenuation of long-range surface plasmon polariton waves," J. Lightwave Technol. **24**, 4391–4409 (2006).
24. O. Tsilipakos, T. V. Yioultsis, and E. E. Kriezis, "Theoretical analysis of thermally tunable microring resonator filters made of dielectric-loaded plasmonic waveguides," J. Appl. Phys. **106**, 093 109 (2009).
25. K. Hassan, J.-C. Weeber, L. Markey, A. Dereux, O. Pitilakis, and E. E. Kriezis, "Thermo-optic plasmo-photonic mode interference switches based on dielectric loaded waveguides," Appl. Phys. Lett. **99**, 241 110 (2011).
26. A. Pitilakis and E. E. Kriezis, "Longitudinal 2x2 switching configurations based on thermo-optically addressed dielectric-loaded plasmonic waveguides," J. Lightwave Technol. **29**, 2636–2646 (2011).
27. J.-C. Weeber, K. Hassan, L. Saviot, A. Dereux, C. Boissière, O. Durupthy, C. Chaneac, E. Burov, and A. Pastouret, "Efficient photo-thermal activation of gold nanoparticle-doped polymer plasmonic switches," Opt. Express **20**, 27 636–27 649 (2012).
28. J. Gosciniak and S. I. Bozhevolnyi, "Performance of thermo-optics components based on dielectric loaded surface plasmon polariton waveguides," Scientific report **3**, 1803 (2013).
29. H. Fan and P. Berini, "Thermo-optic characterization of long-range surface plasmon in Cytop," Appl. Opt. **52**, 162–170 (2013).
30. C. Kittel, *Introduction to solid state physics*,*8th ed.* (John Wiley and Sons, 2005).
31. M. G. Nielsen, J.-C. Weeber, K. Hassan, J. Fatome, C. Finot, S. Kaya, L. Markey, O. Albrektsen, S. I. Bozhevolnyi, G. Millot, and A. Dereux, "Grating couplers for fiber-to-fiber characterizations of stand-alone dielectric loaded surface plasmon waveguide components," J. Lightwave Technol. **30**, 3118–3125 (2012).
32. A. Drezet, A. Hohenau, D. Koller, A. Stepanov, H. Ditlbacher, B. Steiberger, F. R. Aussenegg, A. Leitner, and J. R. Krenn, "Leakage radiation microscopy of surface plasmon polaritons," Mater. Sci. Eng. B **149**, 220–229 (2008).
33. H. Raether, *Surface Plasmons on Smooth and Rough Surface and on Gratings* (Springer-Verlag, Berlin, 1988).
34. N. B. Dahotre and S. P. Harimkar, *Laser Fabrication and Machining of Materials* (Springer, New-York, 2008).
35. J. D. Jackson, *Classical Electrodynamics*, 3rd ed. (John Wiley and Sons, 1999).
36. J.-C. Weeber, A. Dereux, C. Girard, G. Colas des Francs, J. R. Krenn, and J. P. Goudonnet, "Optical addressing at the subwavelength scale," Phys. Rev. E **62**, 7381–7388 (2000).
37. J.-C. Weeber, T. Bernardin, M. G. Nielsen, K. Hassan, S. Kaya, J. Fatome, C. Finot, A. Dereux, and N. Pleros, "Nanosecond thermo-optical dynamics of polymer loaded plasmonic waveguides," Submitted for publication, (2013).
38. G. V. Miloshevsky, V. A. Sizyuk, M. B. Partenskii, A. Hassanein, and P. C. Jordan, "Application of finite difference methods to membrane-mediated protein interactions and to heat and magnetic field diffusion in plasmas," J. Comp. Phys. **212**, 25–51 (2006).
39. R. J. LeVeque, *Finite Difference Methods for Ordinary and Partial Differential Equations* (SIAM,Philadelphia,

#193955 - $15.00 USD Received 15 Jul 2013; revised 30 Aug 2013; accepted 4 Sep 2013; published 13 Sep 2013

2007).
40. M. J. Latif, *Heat Conduction, 3rd ed.* (Springer-Verlag, Berlin Heidelberg, 2009), pp 377.
41. G. Chen and P. Hui, "Thermal conductivities of evaporated gold films on silicon and glass," Appl. Phys. Lett. **74**, 2942–2944 (1999).
42. D. Canchal-Arias and P. Dawson, "Measurement and interpretation of mid-infrared properties of single crystal and polycrystalline gold," Surf. Sci. **577**, 95–111 (2005).
43. P. B. Jonhson and R. W. Christy, "Optical constants of noble metals," Phys. Rev. B **6**, 4370–4379 (1972).
44. W.-J. Lee, J.-E. Kim, H. Y. Park, S. Park, M.-S. Kim, J. T. Kim, and J. J. Ju, "Optical constants of evaporated gold films measured by surface plasmon resonance at telecommunication wavelengths," J. Appl. Phys. **103**, 073 713 (2008).

1. Introduction

Optical properties of metals are known to be temperature-dependent. Thermo-optical properties of metals have been investigated in details several decades ago, mostly for noble metals [1–5]. When a metal is heated, many phenomenons contribute to the change of its dielectric function. A non-exhaustive list of these effects includes electron-electron scattering, electron-phonon scattering, electron-impurity/defect scattering, lattice expansion and/or change in the Fermi distribution [6]. The respective contribution of each of these channels may depend upon the metal, the incident photon frequency, the actual temperature and the amplitude of the temperature change. The temperature-dependent dielectric function of noble metals can be described in the framework of the Drude model [7–9] at least for energies significantly below the interband absorption edge of the metal of interest [9]. An explicit form of this model can be found in refs. [10–12].

The temperature dependence of noble metal optical properties has been reconsidered recently in the context of surface plasmon modes excitation. Indeed, noble metals, are to date the most common materials used to investigate the properties of surface plasmon polariton (SPP) sustained by either extended structures such as thin films or localized structures such as nanoparticles. The thermal properties of nanoparticles have been mainly investigated in the context of localized heat sources relying on resonantly excited nanoparticles (for a recent review see [13]). On the other hand, the impact of temperature onto localized surface plasmon resonances has been also investigated recently for single gold nanoparticles [12], gold nanoparticles embedded into a dielectric matrix [14, 15] and closely packed gold nanorods forming a metamaterial [16]. For crystalline gold nanoparticles, a very good agreement of the experimental data with the results of the temperature-dependent Drude model has been found [12] whereas significant deviations from this model were noticed in the case of evaporated thin films [17, 18]. When excited onto a thin film, SPP modes can be used for bio-sensing purposes and in this respect the role of temperature onto the sensitivity of SPP based sensors has been investigated as well [10, 19]. Thermal modulation of thin film SPPs excited in the Kretschmann-Raether configuration at visible frequencies has also been reported [20, 21]. However, so far, only little has been done to assess quantitatively thermo-optical properties of thin film SPP modes at telecommunication wavelengths (1500nm-1600nm). Beyond a fundamental interest, such a study is needed to characterize the thermo-optical properties of the metal when used as plasmonic waveguides operated in the telecom band.

In this work we focus onto the properties of gold, however the approach we describe in the following can be applied to any metal sustaining SPPs with sufficient propagation length. Many thermo-optic (TO) plasmon-based devices have been reported in the literature recently [22–29]. In these works, the thermo-optic functionality is provided by a high TO coefficient dielectric material whose index is affected by a temperature change which in turn modifies the field distribution of the plasmon mode traveling at the dielectric/metal interface. In these configurations, the TO active part is a dielectric material and so far, except very few works [11], the role of TO

#193955 - $15.00 USD Received 15 Jul 2013; revised 30 Aug 2013; accepted 4 Sep 2013; published 13 Sep 2013

properties of metal in plasmonic structures, at telecom frequencies, has not been considered in details. At telecom wavelengths where gold dielectric function is dominated by free-electron contribution, an increase of the temperature leads to an increase of the ohmic losses through the increase of the electron-phonon scattering rate. In essence, this process is not different from the increase of the static (dc) resistivity of metals for an increasing temperature [30]. The thermally-controlled losses in the metal leads to a SPP mode temperature dependent propagation length which can be used to evaluate the thermo-plasmonic properties of the metal of interest.

The study is organized as follow. We investigate the TO modulation of thin film SPPs traveling at a gold/air interface by operating a specific fiber-to-fiber detection scheme described in the second section. A photo-thermal heating of the metal film is performed by using either a modulated continuous-wave (cw) laser or a nanosecond Q-switched laser. In the third section, we introduce the thermo-plasmonic coefficient of the SPP mode defined as the temperature derivative of the SPP damping constant. We show that this coefficient can be obtained from the experimental depth of modulation of the SPP signal provided that the temperature distribution along the propagation path is known. The computation scheme of the temperature distribution generated by the photo-thermal heating is described in section four along with the procedure leading to the evaluation of gold TOC extracted from the thermo-plasmonic coefficient. Finally, we compare in section five, the thermo-modulation of the SPP signal modeled by using our gold TO coefficients to the experimental depth of modulation produced by a pulsed nanosecond photo-thermal excitation.

2. Experimental set-up

The experimental set-up used for the measurement of SPP photo-thermal modulation is schematically shown in Fig. 1(a). The set-up is built-up around an inverted microscope equipped with an immersion oil objective featuring a large numerical aperture (NA=1.49). The signal collected by the immersion oil objective can be directed either on a visible CCD camera or on a sensitive InGaAs camera. The samples mounted onto the microscope stage are excited at telecom frequencies by a lensed fiber generating a slightly focused spot with a typical radius of 20μm. The input focuser is tilted at an angle of 30° with respect to the optical axis of the microscope. A similar focuser is used for output detection. An arrangement comprising a low numerical aperture long working distance objective is placed above the microscope stage to focus the pump beam (free-space wavelength=532nm). The pump laser can be either a continuous-wave laser modulated by a highly efficient 20ns rise/fall-time electro-optics modulator or a Q-switched laser generating nanosecond pulses. The samples fabricated to investigate photo-thermal modulation of SPP propagation are comprised of a 80nm-thick gold film evaporated onto a 170μm-thick glass substrate. Dielectric input and output grating couplers shown in Fig. 1(b) have been fabricated at the surface of the samples by electron beam lithography using a negative tone resist and following the principles given in ref. [31]. The grating couplers are separated by a distance of 200μm and are excited by an incoherent near-infrared amplified spontaneous source peaked at 1530nm whose spectrum is displayed in Fig. 1(c). The choice of a broadband incoherent light source in the context of this work is dictated by the fact that we want to minimize potential thermally induced changes of the grating coupling efficiency. Indeed, the thermally-induced mismatch with the Bragg condition is expected to be attenuated for a broadband source compared to the case of a highly coherent incident light. The near-infrared signal detected by the output focuser can be directed onto an optical spectrum analyzer (OSA) or a fast (rise time of 2ns) sensitive InGaAs photodiode. The signal of the photodiode is monitored by a 1GHz bandwidth oscilloscope triggered by the signal of the visible photodiode receiving a tiny fraction of the pump beam. The coupling efficiency of the gratings has been characterized by recording the spectrum of the transmitted SPP signal when the input and output focusers are

#193955 - $15.00 USD Received 15 Jul 2013; revised 30 Aug 2013; accepted 4 Sep 2013; published 13 Sep 2013

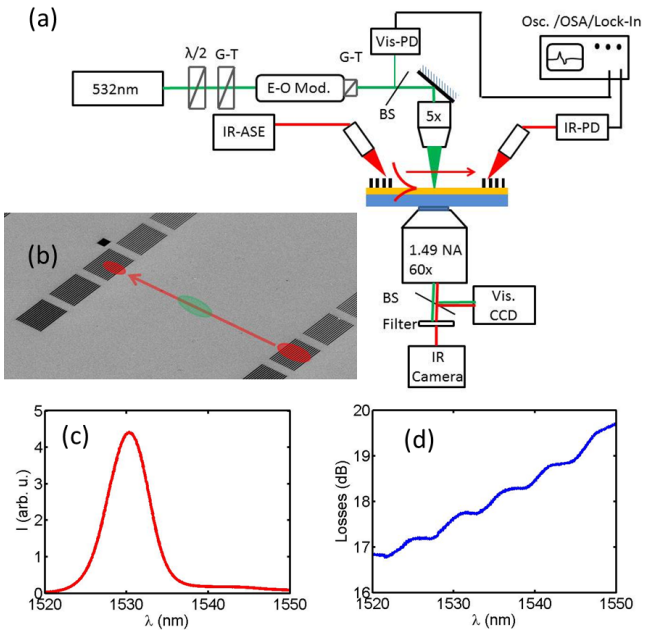

Fig. 1. (a) Schematic view of the experimental set-up. (b) Bird-eye view of the input and output grating couplers implemented at the surface of a thin gold film. (c) Spectrum of the incoherent light-source used for the excitation of the SPP modes. (d) Typical insertion losses for SPP signal fiber-to-fiber transmission.

adjusted at optimum positions on the gratings. This spectrum has been subsequently compared to the reference spectrum obtained by detecting the specular reflection of the incident infrared spot onto a bare gold film area . With this definition of the reference situation, insertion losses including in and out grating coupling losses and SPP propagation losses are below 18dB at 1530nm. We note also that the insertion losses increase with the wavelength indicating that the main contribution to these losses are the coupling losses and not the propagation losses.

Our configuration allows us to record simultaneously leakage radiation (LR) images [32] of a SPP mode traveling between the input and output grating couplers and the corresponding fiber-to-fiber signal. LR images of the gold/air SPP jet excited by the input grating coupler shown on the scanning electron microscope image of Fig. 2(a) are displayed in Figs. 2(b) and (c) with the visible pump being respectively off and on. The illumination of the input grating by the incident spot leads to a SPP jet with a transverse cross-cut of the intensity matching a gaussian profile given by $I(x,y) = I(x,0)\exp\frac{-2y^2}{w_{jet}^2}$ with a waist w_{jet}=9.5μm (see Fig. 2(d)). The pump spot visible onto Fig.2(c) can be observed with the InGaAs camera provided that the long-pass filter placed in front of the camera is removed. In this situation, the visible pump light can be observed with the InGaAs sensor at the expense of a sufficiently long exposure time. By varying the pump beam power and monitoring the resulting signal onto the InGaAs camera, we have verified the linearity of the InGaAs sensor making the use of the InGaAs camera convenient for measurement of the pump spot size. The pump spot shown in Fig. 2(c) and on the inset of Fig. 2(e) corresponds to the pump spot used during the experiments conducted with the cw illumination. As shown in Fig. 2(e), the spot is gaussian with a 16μm half-width at $1/e^2$ of the maximum intensity.

#193955 - $15.00 USD Received 15 Jul 2013; revised 30 Aug 2013; accepted 4 Sep 2013; published 13 Sep 2013

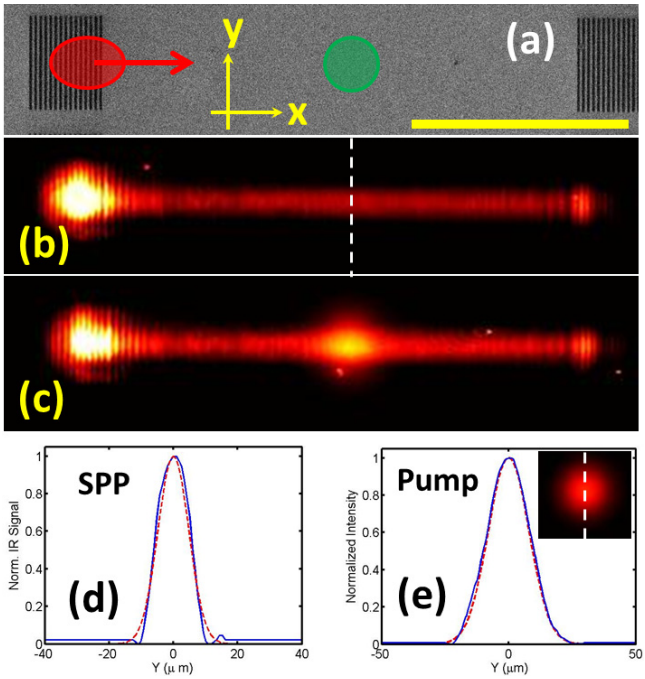

Fig. 2. (a) Scanning electron microscope image of the grating couplers showing the respective location of the input infrared and visible pump spot (scale bar=100μm). (b) (resp.(c)) Leakage radiation image of the SPP jet generated by the input grating coupler with the pump spot off (resp. on). (d) Solid line: Cross-cut of the SPP jet. The jet can be approximated by a gaussian profile (dashed line) with a waist of 9.5μm. (e) Solid-line: Cross-cut of the intensity distribution of the pump spot. The pump spot can be approximated by a gaussian beam (dashed line) with a waist of 16μm.

3. Photo-Thermal modulation of SPP propagation

Figure 3(a) shows the ac coupled SPP signal detected by the InGaAs photo-diode along with the visible photo-diode signal when a photo-thermal cw excitation modulated at a frequency of 1kHz (duty cycle=50%) is applied on the SPP propagation path. For an incident power of 100mW (power of the pump beam measured after the 5x objective and without modulation), the relative depth of modulation $|\Delta I/I|$ is found to be 4.5%. In all the following, the relative depth of modulation is defined as ratio of the SPP signal modulation ΔI during the photo-thermal pumping to the SPP signal I in the cold state in absence of pumping. Knowing the depth of modulation $\frac{\Delta I}{I}$ obtained for known parameters (pump power, pump spot size, plasmon jet width...), a model for SPP propagation modulation is needed to correlate the thermo-optical characteristics of the SPP mode to the experimental value of $\frac{\Delta I}{I}$. We consider the situation depicted in Fig. 3(b). A gold/air plasmon jet centered on the y-axis is traveling along x-axis toward the positive values of x. The plasmon jet has a gaussian transverse profile (along the y-axis) with a waist w_{jet}. We assume that the gold film supporting the SPP mode is locally heated creating a known temperature distribution $T_f(x,y)$ in the plane of the film. More precisely, $T_f(x,y)$ denotes the average temperature of the film over the penetration depth of the SPP mode field. At telecom wavelengths, this penetration depth does not exceed of a few tenths of nanometers. Owing to the vanishing temperature gradient of the gold film over such a thickness,

#193955 - $15.00 USD Received 15 Jul 2013; revised 30 Aug 2013; accepted 4 Sep 2013; published 13 Sep 2013

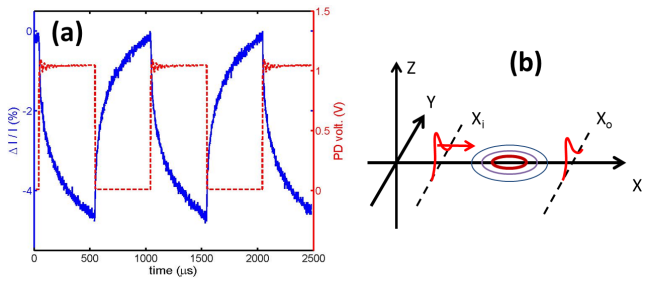

Fig. 3. (a) Solid-line: SPP signal modulation recorded with the IR photo-diode in the case of a photo-thermal excitation with a cw illumination (100mW) modulated at a frequency of 1kHz (duty-cycle=50%). Dashed-line: control signal of the visible photo-diode showing the modulation of the cw pump beam. (b) Schematic view of the SPP jet propagation. The input (resp. output) grating coupler is located at $x = x_i$ (resp. $x = x_o$).

the z dependence for temperature T_f can be safely neglected. For w_{jet} large enough compared to the SPP wavelength, the width of the spatial frequencies spectrum of the plasmon jet can be neglected in the first approximation and the electric field of the SPP jet in the plane of the film verifies:

$$\vec{E}^h(x,y) = \vec{E}^h(x_i,y)\exp(i\Phi(x,x_i,y)) \tag{1}$$

where the superscript h indicates that the film is in the "hot" state. The function $\Phi(x,x_i,y)$ accounts for the accumulation of phase and damping along the distance $(x-x_i)$ and is given by:

$$\Phi(x,x_i,y) = \int_{x_i}^{x} k_{spp}(x',y)dx' \tag{2}$$

The function $k_{spp}(x',y)$ denotes the complex SPP wavevector which depends upon the observation point through the temperature distribution $T_f(x',y)$. The skin depth of gold in the infrared depends linearly on temperature over a range of more than 1000K [2]. Thus, for a sufficiently small temperature change in the range of one or two hundreds of Kelvins, the SPP wave-vector is expected to depend linearly on the temperature as well in such a way that:

$$k'_{spp}(x',y) = k'_{spp} + \partial_T k'_{spp}(T_f(x',y) - T_{room}) \tag{3}$$

and

$$k''_{spp}(x',y) = k''_{spp} + \partial_T k''_{spp}(T_f(x',y) - T_{room}) \tag{4}$$

where k'_{spp} and k''_{spp} are respectively the phase and damping constant of the SPP mode in the "cold" state when the film is at room temperature T_{room} and where $\partial_T k'_{spp}$ and $\partial_T k''_{spp}$ are the partial derivative of respectively the phase and damping constant with respect to the temperature. By introducing equations (3) and (4) into (1), the field at $x = x_o$ can be written:

$$\vec{E}^h(x_o,y) = \vec{E}^h(x_i,y)\exp(i\Phi(x_o,x_i,y)) \tag{5}$$

where $\Phi(x_o,x_i,y)$ is given by:

$$\begin{aligned}\Phi(x_o,x_i,y) &= (k'_{spp} + ik''_{spp})(x_o - x_i) \\ &+ (\partial_T k'_{spp} + i\partial_T k''_{spp}) \int_{x_i}^{x_o} \Delta T(x',y)dx'\end{aligned} \tag{6}$$

#193955 - $15.00 USD Received 15 Jul 2013; revised 30 Aug 2013; accepted 4 Sep 2013; published 13 Sep 2013

where $\Delta T(x',y) = T_f(x',y) - T_{room}$.

For the observation points located along the line $x = x_i$, we assume that the SPP electric field is unaffected by the heating of the film. This assumption is realistic provided that the $x = x_i$ line is located at a sufficiently large distance from the pump spot. With this assumption, we have $\vec{E}^h(x_i,y) = \vec{E}^c(x_i,y)$ where the superscript "c" indicates that the field corresponds to the cold state. By using this last assumption and by noting that $\vec{E}^c(x_o,y) = \vec{E}^c(x_i,y)\exp(i(k'_{spp} + ik''_{spp})(x_o - x_i))$, the electric field in the hot state along the profile $x = x_o$ can be expressed as:

$$\begin{aligned}\vec{E}^h(x_o,y) &= \vec{E}^c(x_o,y) \\ &\times \exp(i\partial_T k'_{spp}\int_{x_i}^{x_o}\Delta T(x',y)dx') \\ &\times \exp(-\partial_T k''_{spp}\int_{x_i}^{x_o}\Delta T(x',y)dx')\end{aligned} \tag{7}$$

From this last equation, the electric field intensity along the profile $x = x_o$ is given by:

$$I^h(x_o,y) = I^c(x_o,y)\exp(-2\partial_T k''_{spp}\int_{x_i}^{x_o}\Delta T(x',y)dx') \tag{8}$$

Experimentally, the signal we record accounts for the intensity distribution of the plasmon jet at the location of the output grating. In this respect, the experimental signal can be approximated by:

$$\frac{\Delta I}{I} = \frac{\int_{-\infty}^{\infty}(I^h(x_o,y) - I^c(x_o,y))dy}{\int_{-\infty}^{\infty}I^c(x_o,y)dy} \tag{9}$$

Given that the argument of the exponential term in equation (8) is expected to be small, the depth of modulation $\frac{\Delta I}{I}$ can be expressed as:

$$\frac{\Delta I}{I} = \frac{-\int_{-\infty}^{\infty}I^c(x_o,y)(2\partial_T k''_{spp}\int_{x_i}^{x_o}\Delta T(x',y)dx')dy}{\int_{-\infty}^{\infty}I^c(x_o,y)dy} \tag{10}$$

The plasmon jet having an intensity gaussian distribution along the y-axis, the cold state intensity can be written:

$$I^c(x_o,y) = I_0\exp(-2k''_{spp}x_o)\exp(\frac{-2y^2}{w_{jet}^2}) \tag{11}$$

By introducing $I^c(x_o,y)$ into equation (9) and using Gauss integrals, we find that the experimental depth of modulation is related to the temperature derivative of the damping constant of the SPP mode by:

$$|\frac{\Delta I}{I}| = 2\partial_T k''_{spp}\int_{x_i}^{x_o}\Delta T_{av}(x')dx' \tag{12}$$

where the average change of temperature is given by:

$$\Delta T_{av}(x') = \int_{-\infty}^{\infty}\sqrt{\frac{2}{\pi w_{jet}^2}}\exp(\frac{-2y^2}{w_{jet}^2})\Delta T(x',y)dy \tag{13}$$

We emphasize that this approach holds for temperature ranges such that the SPP effective index depends linearly on temperature and for a collimated plasmon jet with a gaussian transverse intensity profile. On the basis of this analysis, we conclude that the temperature derivative of the SPP mode damping constant, denoted hereafter as the thermo-plasmonic coefficient, can be extracted from the experimental depth of modulation provided that the temperature distribution along the thin film is known. Note that, so far, only the thermo-plasmonic coefficient can be obtained with this approach. In order to correlate this SPP mode property to the thermo-optical properties of gold, further developments are necessary.

#193955 - $15.00 USD Received 15 Jul 2013; revised 30 Aug 2013; accepted 4 Sep 2013; published 13 Sep 2013

4. Thermo-optical coefficients of gold at telecom frequencies

4.1. Gold TO coefficients characterization from gold/air SPP thermo-modulation

We have shown in the previous section that the thermo-plasmonic coefficient $\partial_T k''_{spp}$ can be obtained from the SPP thermo-modulation depth if the temperature distribution along the film is known. However, in order to correlate this parameter to the thermo-optical properties of gold, we need to analyze in more details the properties of gold/air interface SPP at telecom frequencies. For a gold film thick enough to neglect radiation losses compared to intrinsic losses, the wave-vector of a gold/dielectric interface SPP can be approximated by [33]:

$$k_{spp} \simeq k_0 \sqrt{\frac{\varepsilon_m \varepsilon_d}{\varepsilon_m + \varepsilon_d}} \tag{14}$$

where ε_m and ε_d are respectively the dielectric function of gold and of the dielectric medium in contact with gold (air in our case), and where $k_0 = \frac{2\pi}{\lambda_0}$, with λ_0 the free-space wavelength of the incident light. At telecom frequencies, the absolute value of ε'_m, the real part of the dielectric function of gold, is much larger than the imaginary part ε''_m. In addition, if $|\varepsilon'_m|$ is also much larger than ε_d, the attenuation constant of the SPP mode traveling at the metal/dielectric interface can be approximated by:

$$k''_{spp} = \Im(k_{spp}) \simeq \frac{\varepsilon_d^{3/2} k_0}{2} \frac{\varepsilon''_m}{(\varepsilon'_m)^2} \tag{15}$$

The complex dielectric function ε_m is related to the complex refractive index of gold through the relation $\varepsilon_m = (n + i\kappa)^2$ where n and κ are respectively the real refractive index and the extinction coefficient of gold. At telecom frequencies, κ is typically more than ten times larger than n in such a way that the real dielectric function can be approximated by $\varepsilon'_m = (n^2 - \kappa^2) \simeq -\kappa^2$. By using this approximation and by taking the temperature derivative of the attenuation constant given by equation (15), we find:

$$\partial_T k''_{spp} = \frac{\varepsilon_d^{3/2} k_0}{\kappa^3} (\partial_T n - \frac{3n}{\kappa} \partial_T \kappa) \tag{16}$$

Note that this last equation holds only if the dielectric function ε_d is only marginally affected by the heating of the gold film, a condition that is expected to be fulfilled when the SPP mode is traveling at the interface between gold and air. Note also that equation (16) indicates that if temperature derivatives $\partial_T n$ and $\partial_T \kappa$ are of same order of magnitude, the main contribution to $\partial_T k''$ comes from the TOC for the real refractive index of gold since the ratio $\frac{3n}{\kappa}$ is of the order of 10% for gold in the infrared. If the unknown $\partial_T n$ and $\partial_T \kappa$ are the quantities of interest, a second equation, in addition to equation (16), is necessary to compute the two TOCs. This second equation is provided by the experimental data reported in ref. [1] where the change of complex dielectric function of gold have been investigated for temperatures ranging from 295K to 770K. The same data have been used to extract gold TOC over the visible range in ref. [14] at the cost however of a Kramer-Kronig analysis. In our case, the experimental data from ref. [1] are used to evaluate the temperature derivative $\partial_T \varepsilon''_m$ which is needed in conjunction with equation (16) to extract gold TOC given that:

$$\partial_T \varepsilon''_m = 2\kappa \partial_T n + 2n \partial_T \kappa \tag{17}$$

In summary, gold TOC can be computed by using equations (16) and (17) provided that $\partial_T k''_{spp}$ and $\partial_T \varepsilon''_m$ are known. However, according to equation (12), the thermo-plasmonic coefficient $\partial_T k''_{spp}$ can be evaluated from the measurement of the modulation depth $\frac{\Delta I}{I}$ only if the temperature distribution of the gold film is known. The approach we use for the computation of this temperature distribution is described in the next paragraph.

#193955 - $15.00 USD Received 15 Jul 2013; revised 30 Aug 2013; accepted 4 Sep 2013; published 13 Sep 2013

4.2. *Temperature distribution of the gold film under modulated cw illumination*

The problem of computing the temperature distribution in a bulk metal under a laser irradiation is of key importance in fields such as laser machining for example. Usually, the situation is reduced to a one-dimensional heat diffusion problem leading to an analytical solution [34]. In our case, we rely on a numerical approach in order to avoid an oversimplification of the system. Owing to the cylindrical symmetry of a gaussian beam impinging at normal incidence onto

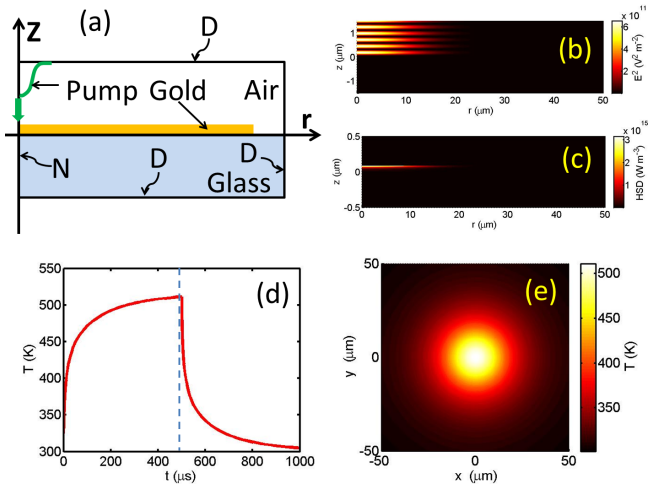

Fig. 4. (a) Schematic view of the system considered for the finite-difference computation of the temperature distribution along the gold thin film under photo-thermal excitation. The computation window is 100μm long (along r coordinate) and 50μm high (in the Z direction). A Neumann (N) boundary condition $\frac{\partial T}{\partial r} = 0$ is applied at $r = 0$ due to the rotational symmetry around Z-axis whereas Dirichlet (D) conditions $T = T_{room}$ are used for the three other boundaries. (b) Electric intensity distribution of the interference pattern created by the interaction of the normally incident and back-reflected pump beams. The power carried by the incident beam is 100mW. (c) Heat-source density distribution corresponding to the electric intensity distribution shown in (b). (d) Temperature in the thin film at the focal point of the gaussian beam as a function of time in the case of a 1kHz modulation frequency (duty-cycle=50%). (e) Spatial temperature distribution at the surface of the thin film at t=500μs.

an infinitely extended thin film, we consider the situation depicted in Fig. 4(a). In cylindrical coordinates the time-dependent heat diffusion equation can be written:

$$\rho C_p \frac{\partial T}{\partial t} = \frac{1}{r}\frac{\partial}{\partial r}(rk\frac{\partial T}{\partial r}) + \frac{\partial}{\partial z}(k\frac{\partial T}{\partial z}) + \tilde{Q}_E(r,z) \tag{18}$$

where ρ, C_p and k are position dependent functions representing respectively the density, the specific heat and the thermal conductivity of the different materials in the system. The source term $\tilde{Q}_E(r,z)$ corresponds to a volume power density and is denoted in all the following as the heat source density (HSD). In our case, the HSD is generated by the ohmic losses of the pump beam into the metal film. The HSD or in other words the amount of energy converted into heat in the film per unit time per unit volume is given by [35]:

$$\tilde{Q}_E(r,z) = \frac{1}{2}\Re(\vec{J}(r,z).\vec{E}^*(r,z)) \tag{19}$$

#193955 - $15.00 USD Received 15 Jul 2013; revised 30 Aug 2013; accepted 4 Sep 2013; published 13 Sep 2013

where $\vec{J}$ is the current density and where $\Re$ denotes the real part. By using Ohm's law, the heat source density can be more conveniently written in our situation:

$$\tilde{Q}_E(r,z) = n\kappa \frac{k_0}{Z_0} |E(r,z)|^2 \tag{20}$$

where Z_0 is the vacuum impedance and where $n+i\kappa$ is the complex refractive index of gold at the pump frequency for observation points located within the thin gold film. The HSD can be readily computed by using a plane wave expansion of the incident pump beam [36]. Figure 4(b) shows the electric field intensity distribution of a gaussian beam expanded over up to 430 plane-waves (λ_0=532nm, beam waits=16μm) carrying a total power of 100mW. Although not necessary for a system comprised of a bare thin film deposited onto a substrate, the plane wave expansion of the gaussian beam becomes very convenient to account for the presence of a surface defect on top of the thin film [37]. The electric field for observation points within the metal film is obtained from this plane wave expansion and eventually the HSD is computed according to equation (20). Figure 4(c) shows the HSD corresponding to the pump beam falling onto a 80nm-thick gold film. As expected, the HSD features a strong decay along the direction perpendicular to the thin film as a result of the 35nm skin depth for gold at 532nm. The HSD spatial distribution is next used as an input for solving the heat diffusion equation (18). We use an implicit centered finite difference scheme implemented on a non-regular rectangular mesh [38, 39] in order to compute the temperature distribution at all observation points within the computation windows (see caption of Fig. 4). At this stage, the value for the thermal conductivity k of the gold film must be chosen carefully as it impacts both the transient properties and the steady-state temperature distribution of the gold film. It is known that for metal thin films with a thickness of the order of the electrons mean free path, the classical size effect [40] reduces significantly heat conductivity compared to bulk materials. For example, for bulk gold k is tabulated at 317 W.m^{-1}.K^{-1} whereas in the case of films with a typical thickness around 100nm, thermal conductivity as low as k =120 W.m^{-1}.K^{-1} have been obtained [41]. The ratio of the bulk conductivity k_b to the thin films conductivity k is given by [41]:

$$\frac{k_b}{k} = 1 + \frac{3}{8t} + \frac{7\alpha}{5} \tag{21}$$

where $t = \frac{d}{l}$ and $\alpha = \frac{l}{D}(\frac{R}{1-R})$ with d the film thickness, l the electron's mean free path, D the average grain size in the film and R the grain boundary reflection coefficient. These parameters have been specifically investigated for gold in the mid-infrared in ref. [42]. For polycrystalline thin films, typical values for l and R are 17nm and 0.63 respectively. High magnification scanning electron microscope characterization (not shown) reveals that the average grain size for our 80nm-thick films is about D=65$\pm$6nm leading to a heat conductivity for our gold films of k =150W.m^{-1}.K^{-1}. By using this value, the temperature at the surface of the thin film at the focal point ($r=0, z=0$) of the pump beam shown in Fig. 4(d) has been obtained for an incident (dc) power of 100mW modulated at a frequency of 1 kHz with a duty-cycle of 50%. The spatial distribution of the temperature in the plane of the thin film at t =500μs right before the end of the heating cycle is shown in Fig. 4(e). Knowing the temperature distribution in the film, we can extract first, the thermo-plasmonic coefficient $\partial_T k''_{spp}$ and second, the TOC of gold at telecom wavelengths.

4.3. Thermo-plasmonic figure of merit and gold TOC at telecom frequencies

The effective computation of gold TOC is conducted by considering the experimental situation where the pump beam has a power of 100mW. When modulated at 1kHz with a duty-cycle of 50%, the photo-thermal modulation of the SPP signal traveling through the heated area

#193955 - $15.00 USD Received 15 Jul 2013; revised 30 Aug 2013; accepted 4 Sep 2013; published 13 Sep 2013

leads to a modulation depth of $|\frac{\Delta I}{I}| = 4.5\%$ (see Fig. 3(a)). From this modulation depth and the temperature distribution along the thin film at the end of the heating period (t =500μs), we evaluate (from equation (12)) the thermo-plasmonic coefficient $\partial_T k''_{spp}$ of the gold/air SPP mode at 2.90×10^{-6} μm^{-1}.K^{-1}. Next, for the reference situation we consider (pump beam power of 100mW), the maximum temperature of the film at the end of the heating period is around 510K. Thus, the temperature derivative $\partial_T \varepsilon''$ for the gold film is expected to be 0.01425 K^{-1} according to the results reported in ref. [1] for temperatures ranging from 470 to 670K. Knowing both $\partial_T k''_{spp}$ and $\partial_T \varepsilon''$, the TO coefficients of the gold film can be obtained from equations (17) and (16) provided that the refractive index of gold at room temperature is known. In all the following we use a complex refractive index of gold of $0.515 + i10.65$ extracted from tabulated values reported in ref. [43] for a free-space wavelength of 1.53μm. This choice is motivated by the fact that the refractive index of gold thin films was measured at telecom frequencies [44] and found to be in good agreement with the values reported in ref. [43]. For example, at a free space wavelength of 1.55μm, the refractive index of thin films with a typical thickness around 60nm was measured at 0.505+i10.7 deviating by less than 3% for n and κ compared to the value 0.52+i10.8 reported in ref. [43]. Given the refractive index of gold at room temperature, the linear system formed by equations (17) and (16) can be solved for $\partial_T n$ and $\partial_T \kappa$ leading to TO coefficients displayed in Table 1. Our TO coefficients are compared to the linear TO coefficients obtained from the temperature-dependent Drude model for gold described in ref. [11]. Although of same order of magnitude, we note however that our TO coefficients are significantly different from those given in ref. [11]. In particular, $\partial_T n$ is more than two-fold smaller in our case as compared to the model developed in ref. [11]. Actually, our values compare more favorably with the linear extrapolation at 1.53μm of the gold TOC (obtained from the Kramer-Kronig analysis of ref. [1] data) given in ref. [14] at a wavelength of 1.24μm.

Table 1. Comparison of the thermo-optical coefficients of gold extracted from the measured SPP depth of modulation and from the temperature-dependent Drude model for gold given in ref. [11]. The results of ref. [14] are obtained from a linear extrapolation (see text).

TO coeff.	$\partial_T n$ (K^{-1})	$\partial_T \kappa$ (K^{-1})
This work	0.72×10^{-3}	-1.0$\times10^{-3}$
Ref. [11]	1.68×10^{-3}	-0.32$\times10^{-3}$
Ref. [14]	0.55×10^{-3}	-1.78$\times10^{-3}$

Figure 5(a) shows the modulation depth computed from equation (12) by using either our TO values or the model of ref. [11] for different incident peak power pump beam modulated at 1kHz with a 50% duty cycle. Whatever the incident pump power, the temperature-dependent Drude model for gold leads to a depth of modulation which is overestimated by about 60% compared to our experimental values or computed values. The experimental oscilloscope traces of the

#193955 - $15.00 USD Received 15 Jul 2013; revised 30 Aug 2013; accepted 4 Sep 2013; published 13 Sep 2013

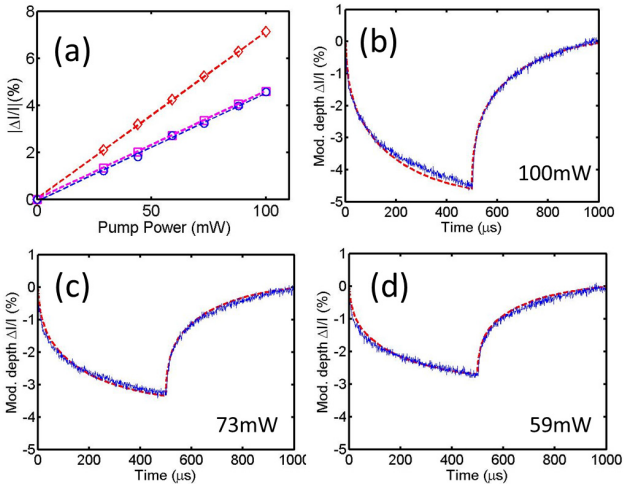

Fig. 5. (a) Comparison of the experimental modulation depth (open circles) and the modulation depth computed using either our values for gold TOC (open squares) or the temperature-dependent refractive index given in ref. [11] (open diamonds). (b) (resp. (c) and (d)) Comparison of the experimental (solid line) and computed SPP modulation (dashed line) as a function of time in the case of a modulated cw excitation (1kHz, duty-cycle=50% for an incident power of 100mW (resp. 73mW and 59mW).

thermo-modulated SPP signal displayed in Fig. 5(b)-(d) are compared to the modeled traces computed by using our gold TOC values. Apart for a small deviation for times larger than $200\mu s$ after the beginning of the heating cycle and for an incident power of 100mW, we observe a quite good agreement between the computed and experimental profiles suggesting that our computations allow us to extract not only the amplitude of the photo-thermal modulation but also the characteristic time for this modulation. Although of great practical importance, the dynamic of photo-thermal SPP modulation is however out of the scope of the present work and is analyzed in details down to the nanosecond regime for confined plasmonic waveguides in ref. [37].

When considering the results displayed in Fig. 5(a), it is worth to comment on the amplitude of the SPP signal photo-thermal modulation. We have found that a temperature rise as large as 200K (for a pump power of 100mW) generates a SPP modulation amplitude as small as 4.5%. This result can be understood from the fact that the gold/air interface mode we consider is only very little confined within the metal and thus features a long propagation distance and accordingly a weak thermo-plasmonic $\partial_T k''_{spp}$ coefficient. For SPP modes with losses dominated by ohmic losses (bounded or a weakly leaking modes), the damping constant $L_{spp} = \frac{1}{2k''_{spp}}$ is inversely proportional to the SPP field confinement into the metal. In this respect, the quantity $L_{spp} \times \partial_T k''_{spp}$ can be viewed as a figure of merit (FOM) characterizing the thermo-optical sensitivity of the metal for plasmonic applications at a given frequency. Relying on the modulation obtained for the pump power of 100mW, we find in our case a FOM for gold at telecom wavelengths of:

$$L_{spp} \times \partial_T k''_{spp} = 8.0 \times 10^{-4}\, K^{-1} \tag{22}$$

where L_{spp} =$276\mu m$ calculated for the gold/air SPP mode has been used to evaluate the numerical value of the FOM. As long as thermal modulation of surface plasmon modes is concerned, the use of the FOM defined above is an interesting practical approach. Indeed, knowing this

#193955 - $15.00 USD Received 15 Jul 2013; revised 30 Aug 2013; accepted 4 Sep 2013; published 13 Sep 2013

FOM from measurements performed on a given SPP mode, one can obtained at least a coarse evaluation of the thermo-modulation depth for an other SPP mode provided that the propagation distances for the two modes are known in the cold state. For example, by using our gold TOC values, we calculate that the depth of modulation for the glass/gold interface SPP mode (L_{spp}=81μm) should be around 14.6% when the pump power is 100mW. For the same excitation conditions, this depth of modulation is evaluated at 15.3% when the calculation is performed by using the FOM value for gold given above.

5. Photo-thermal SPP modulation in the nanosecond regime

The TO coefficients of gold have been obtained from the measurements of the SPP signal thermo-modulation created by a modulated cw source. The goal of this last section is to test the reliability of our gold TOC values in the context of a nanosecond pulsed illumination. The experiments of this last section have been performed simply by replacing the cw laser and the electro-modulator shown in Fig. 1 by a 532nm Q-switched laser. The laser has a repetition rate of 8.3kHz and delivers 6.5μJ pulses with a width (full width at half maximum) of 0.59ns as specified by the manufacturer. In all the following, we assume that the pulses have a gaussian temporal profile. In order to prevent thin film damaging, the pump spot has been enlarged compared to the case of cw excitation. As shown in Figs. 6(a) and (b), the pump spot we use now has a gaussian spatial profile with a waist of 50μm. Figure 6(c) shows the oscilloscope

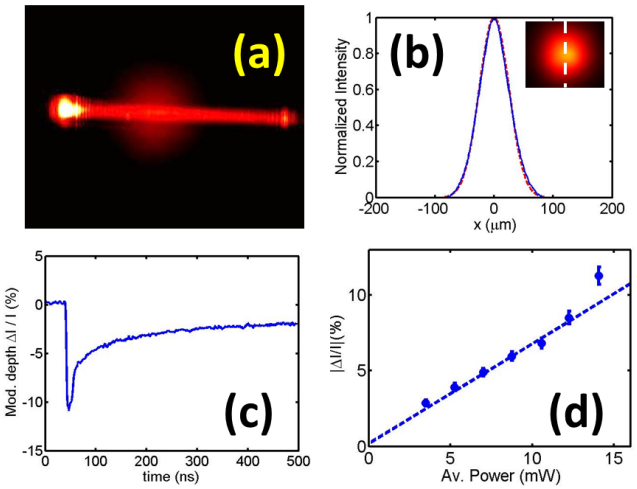

Fig. 6. (a) Leakage radiation image showing the infrared plasmon jet and the nanosecond pump spot. (b) Optical image of the pump spot. The experimental intensity profile (solid line) of the pump beam is close to a gaussian beam (dashed line) with a waist of 50μm. (c) Oscilloscope trace showing the modulation of the SPP signal under excitation with the Q-switched nanosecond laser. The average power is 14mW. (d) Depth of modulation of the SPP signal as a function of the average power of the pulsed pump beam.

trace of the SPP signal recorded for an average pump power of 14mW. The modulation of the SPP signal exhibits an asymmetric shape with an amplitude of 11.7% resulting from the abrupt rise of the film temperature over the duration of the pulse and the much slower cooling after the end of the pulse. Figure 6(d) displays the modulation depth $\frac{\Delta I}{I}$ as a function of the average pump power. Note that these experiments were conducted by increasing the pump power meaning that low pump powers were investigated first. The modulation depth depends

#193955 - $15.00 USD Received 15 Jul 2013; revised 30 Aug 2013; accepted 4 Sep 2013; published 13 Sep 2013

linearly on the pump power until a threshold around 12.2mW whereas the point obtained for 14mW departs significantly from the linear behavior. This result is attributed to a change of the structural properties of the metal film. This conclusion has been confirmed by a subsequent electron microscope characterization showing a clear change of the grain size of the film at the location of the pump spot center indicative of a possible partial melting of the film in this area. Disregarding the result obtained at 14mW, we obtain a modulation efficiency corresponding to the slope of the linear fit displayed in Fig. 6(d) of 0.66 %.mW^{-1}.

The evaluation of the SPP depth of modulation requires the computation of the temperature distribution in the system at any time during the pulsed illumination. For nanosecond pulses illuminating a metal, the free-electron gas and the lattice are at thermal equilibrium after a characteristic time (10ps) much shorter than the pulse duration. In this respect a two-temperatures model (accounting for a temperature of the electron gas different from the ion lattice temperature) is usually not necessary in the pulsed nanosecond regime and the computation of the temperature can be conducted following the same procedure described for cw excitation. Figure 7(a) shows the temporal change of the gold film temperature at the center of the pump beam for an incident average power of 12.2mW. The instantaneous power of the pump pulse for such an average power is displayed in the inset of Fig. 7(a). The heat source density resulting from

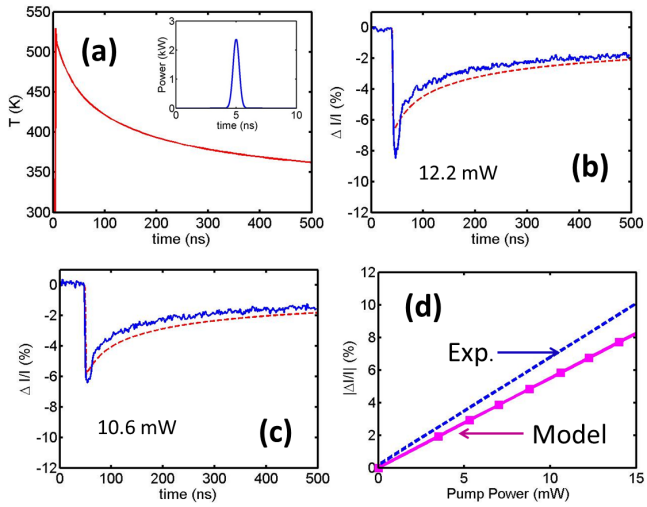

Fig. 7. (a) Temperature of the thin film at the center of the pump beam in the case of an incident pulse with an average power of 12.2mW a repetition rate and a pulse duration corresponding to the experimental situation. The incident pulse reaches its maximum at t=5ns as shown on the inset displaying the power of the pulse as a function of time. (b) (resp. (c)) Comparison of the experimental (solid line) and computed (dashed line) SPP photo-thermal modulation for an average incident power of 12.2mW (resp. 10.6mW). The computed profile accounts for the 2ns rise time of the infrared photo-diode response. (d) Comparison of the experimental (dashed line) depth of modulation and the depth of modulation (solid line) computed using our gold TOC values.

the absorption of the pump beam follows the temporal profile of the incident pulse and thus the temperature rises over the pulse duration but decays at a rate controlled by the characteristic time for heat dissipation in the system. Knowing the temperature distribution at each time, the depth of modulation is computed according to equation (12) with the thermo-plasmonic coefficient given by equation (16). The experimental and computed temporal profiles are su-

#193955 - $15.00 USD Received 15 Jul 2013; revised 30 Aug 2013; accepted 4 Sep 2013; published 13 Sep 2013

perimposed on Fig. 7(b) and (c) for incident powers of 12.2mW and 10.6 mW respectively. In both cases, we note that modulation depths computed with our gold TOC values are slightly under-estimated compared to the experimental values. The computed modulation efficiency is compared to the experimental one in Fig. 7(d). As expected, the computed depth of modulation increases linearly with the pump power, at a rate of $0.55\%.mW^{-1}$, smaller by about 17% compared to the experimental rate. Such a discrepancy could be related to a pulse duration (which could not be measured experimentally due to the rise time of our visible photo-diode) slightly different than the specification. A more accurate modeling of temperature distribution including a temperature-dependent absorption of gold film at the pump wavelength could also contribute to a better agreement between computed and experimental pulsed SPP thermo-modulation. Nevertheless, in spite of this difference, we note that the thermo-plasmonic properties of SPP modes supported by gold at telecom frequencies can be predicted with a fairly good accuracy by using the TO coefficients obtained in this work.

6. Conclusion

In summary, we have investigated the photo-thermal modulation of thin film SPP mode launched at a gold/air interface at telecom frequencies by operating a specific fiber-to-fiber detection configuration in conjunction with a leakage radiation microscope set-up. For a gold/air SPP mode at telecom frequencies, we have shown that the depth of modulation is proportional to the thermo-plasmonic coefficient defined as the temperature derivative of the damping constant of the mode. This coefficient has been obtained in the case of a gold/air SPP mode by using the experimental depth of modulation and the temperature distribution along the film computed by means of a finite-difference scheme. Next, we have proposed a figure of merit which can be useful to characterize the thermal properties of a metal at a given wavelength. Once established on the basis of the thermo-modulation of a given SPP mode, the figure of merit can be conveniently used for a rough evaluation of the thermo-plasmonic properties of other SPP modes. By using our experimental results in conjunction with optical data available in the literature, we have computed the thermo-optical coefficients of gold at telecom wavelengths. These coefficients lead to a SPP thermo-modulation amplitude about 60% lower than predicted by the temperature-dependent Drude model for gold. We have checked the reliability of our gold TOC by performing photo-thermal experiments with a pulsed nanosecond laser. Although the computed depth of modulation for pulsed illumination are underestimated by about 17% compared to the experimental values, we conclude that the gold TOC obtained in this work are reasonable and can be useful for anticipating thermal effects on SPP modes supported by gold at telecom wavelengths. The next steps in the study of SPP mode photo-thermal control include the characterization of the temporal dynamic of the modulation in the case of plasmonic waveguides featuring a high field confinement and the use of pulsed photo-thermal excitation for the activation of fast thermo-plasmonic devices.

Acknowledgments

This work has benefited from the financial support of the Agence Nationale de la Recherche through the P2N program project MASSTOR (Grant number ANR-11-NANO-022).

#193955 - $15.00 USD Received 15 Jul 2013; revised 30 Aug 2013; accepted 4 Sep 2013; published 13 Sep 2013